Earth and Planetary Science Letters 345-348 (2012) 38–48

Contents lists available at SciVerse ScienceDirect

Earth and Planetary Science Letters

journal homepage: www.elsevier.com/locate/epsl

Letters

Solubility of molecular hydrogen in silicate melts and consequences for volatile evolution of terrestrial planets

M.M. Hirschmann *, A.C. Withers, P. Ardia, N.T. Foley

Department of Earth Sciences, University of Minnesota, Minneapolis, MN 55455, USA

ARTICLE INFO

Article history:
Accepted 14 June 2012
Editor: L. Stixrude
Available online 20 July 2012

Keywords:
Hydrogen
lunar water
nebular atmosphere
H in core deep melting

ABSTRACT

We present experiments from 0.7 to 3 GPa that quantify solubility of H_2 in silicate melts under controlled hydrogen fugacities (f_{H2}). Two experimental series, one on synthetic basalt+COH and other with a synthetic andesite+OH, were conducted using a double capsule technique to impose a range of f_{H2}, on the samples. Quenched glasses were analyzed by FTIR and SIMS. Both series follow simple solubility laws in which molecular H_2 concentrations are proportional to f_{H2} and with a partial molar volume of molecular H_2 of 11 cm^3/mole. Solubilities in andesitic melt are systematically greater than in basaltic liquid in a relationship consistent with control by the ionic porosity (IP) of the melts. Extrapolation based on IP allows estimation of the solubility of H_2 in peridotitic melts applicable to magma oceans. The $H_2/(H_2+H_2O)$ ratio in silicate melts (where H_2O includes molecular H_2O and OH^-) increases as conditions become more reduced, with increasing pressure, and with increasing total H. Under some conditions prevailing in the early Earth and terrestrial planets as well as in the deep Earth today, H_2 can be a significant fraction of the dissolved H and at high pressure it may exceed "water" (H_2O and OH^-). Therefore, magmatic H_2 may influence the initial distribution of volatiles and the redox evolution of terrestrial planets, as well as the ongoing formation and fate of hydrous melts in the deep Earth today. Hydrous species in melts in equilibrium with Fe-rich alloy at high pressure, for example during core formation from a magma ocean, could be chiefly H_2, rather than H_2O. Hence, delivery of H_2 to the core by removal of Fe hydride need not be coupled to oxidation of the residual mantle. Although lunar basalts are much reduced, the fraction of H dissolved as molecular H_2 is small owing to low total H concentrations. Extrapolation to conditions of potential hydrous partial melting in the deep Earth suggests that the chief magmatic volatile may be H_2 rather than H_2O. The very small partial specific density of magmatic H_2 (0.18 g/cm^3 at low pressure) may provide significant positive buoyancy to deep partial melts.

1. Introduction

The behavior of magmatic volatiles has a key influence on a broad spectrum of processes in Earth and planetary sciences, including the composition of planetary mantles, cores, and exospheres, the locus of partial melting in the mantle and crust, the fate of those partial melts and their role in geochemical differentiation, the evolution of planetary atmospheres and maintenance of equable climates and planetary habitability, the explosivity of volcanic eruptions, and more. H_2O and CO_2 are the principle volatile components in terrestrial magmas, and so their behavior, including solubilities and influences on magmatic processes, has been studied intensively. However, highly reducing conditions may prevail in several important environments, including those in the earliest Earth (Rubie et al., 2011), those on other terrestrial bodies such as the Moon and Mars (Sato, 1976; Karner et al., 2006; Wadhwa, 2008;,), and deep in the Earth today (Frost and McCammon, 2008). In these environments, molecular hydrogen could be an important magmatic species. Yet, studies of reduced volatiles in magmas remain limited and determinations of concentration and influence of molecular hydrogen, H_2, in reduced magmas are sparse.

During planetary accretion and differentiation, the distribution of C–O–H volatiles between the cores, mantles, and atmospheres of terrestrial planets is mediated by dissolution in magma oceans. Early planetary atmospheres formed from nebular gas are nearly pure hydrogen, and those from degassing of impacting planetesimals may also be hydrogen-rich (Schaefer and Fegley, 2007; Hashimoto et al., 2007). Dissolution of hydrous components in magma oceans modulates the proportions remaining in early atmospheres and potentially delivers significant H to the mantles and cores of growing terrestrial planets.

* Corresponding author.
E-mail addresses: mmh@umn.edu, marc.m.hirschmann-1@umn.edu (M.M. Hirschmann).

0012-821X/$ - see front matter © 2012 Elsevier B.V. All rights reserved.
http://dx.doi.org/10.1016/j.epsl.2012.06.031

Recent discoveries demonstrate that lunar magmas contain a modest hydrous component (Saal et al., 2008; Boyce et al., 2010; Greenwood et al., 2011; McCubbin et al., 2010a; Hauri et al., 2011), though the absolute concentrations of H in the lunar interior remain uncertain. Oxybarometry indicates oxygen fugacities prevailing in lunar magmas are between those equivalent to coexistence of iron and wüstite (IW) and 2 log units below (IW-2) (Karner et al., 2006; Wadhwa, 2008). Under these conditions, C–O–H vapors are rich in H_2 (e.g., Holloway and Blank, 1994). Consequently, H_2 could be an important lunar volatile (Elkins-Tanton and Grove, 2011). Martian magmas also contain a hydrous component (McCubbin et al., 2010b) and also are in some cases quite reduced, with oxygen fugacities as low as IW-0.7 (Wadhwa, 2008).

Igneous materials from the Earth's crust and shallow mantle are comparatively oxidized, such that H_2O and CO_2 are the dominant C–O–H volatile species (Holloway and Blank, 1994). Geochemical evidence suggests that this has been so at least for the last 3.9 Ga (Delano, 2001) and possibly as far back as 4.4 Ga (Trail et al., 2011). However, with increasing depth, stabilization of Fe^{3+} in high pressure phases produces reducing conditions, such that FeNi metal alloy precipitates in the deep upper mantle (Rohrbach et al., 2007; Frost and McCammon, 2008). Oxygen fugacities at 400 km are close to the IW buffer (Frost and McCammon, 2008) and in the lower mantle, saturation with nearly pure Fe alloy produces oxygen fugacities below IW-1 (Frost et al., 2004). Deep hydrous melts, such as those that may form above the 410 km discontinuity, as posited by the transition zone water filter (TZWF) model (Bercovici and Karato, 2003) and imaged seismically (e.g., Tauzin et al., 2010), therefore form in a reducing environment, where $H_2 \pm CH_4$ may be important volatiles in addition to or instead of $H_2O \pm CO_2$. Constraints on the abundance of these reduced volatiles in deep magmas, as well as their influence on the stability and properties of the magmas are scarce.

Several studies have documented dissolved molecular H_2 in silicate liquids or glasses under reducing conditions. Quantitative studies of H_2 solubility using FTIR have included one study on obsidian glass at 800 °C and low H_2 gas pressures ($\leq$70 bar) (Gaillard et al., 2003), and one on pure SiO_2 glass at 800–955 °C and 0.2 GPa (Schmidt, 1998). Most other studies (Luth et al., 1987; Kadik et al., 2004, 2011; Mysen et al., 2011) have relied chiefly on Raman spectroscopy, which allows characterization but not quantification of the H_2 species. Two recent studies reported H concentrations from experimentally quenched liquids for which spectroscopic examination revealed significant molecular H_2. These studied the solubility of N–O–H (Mysen et al., 2011) and N–C–O–H species (Kadik et al., 2011) in silicate melts, respectively, and determined H concentrations with analytical techniques that do not distinguish between molecular H_2 and other hydrous species (OH^-, H_2O, CH_4, NH_3, etc.). So, although molecular H_2 is known to be present in glasses quenched from reduced conditions, concentrations and their dependence on intensive variables are poorly understood.

Here we determine H_2 solubilities in basaltic and andesitic liquids at high pressure and over a range of fixed hydrogen fugacities. These represent the first systematic quantification of the concentrations of dissolved molecular H_2 in aluminosilicate melts.

2. Methods

We conducted two series of hydrogen solubility experiments, one with a molten synthetic basalt coexisting with C–O–H fluids and a second with molten synthetic andesite coexisting with nominally C-free O–H fluids. Experiments were conducted at pressures from 0.7 to 3 GPa and at 1400–1500 °C, and fixed f_{H2} were imposed with a double capsule technique (Table 1).

Table 1
Experimental conditions and notes on textures.

Experiment	P (Gpa)	T (°C)	t (min)	Outer capsule buffer[a]	Glass	Notes[b]
Series 1 Basalt+C–O–H						
B343	0.7	1400	30	IW	Clear	Si,B
A812	1.5	1400	30	IW	Clear	Si,B
B337	1.5	1400	60	IW	Clear	Si,B
A697	1.5	1450	120	IW	Clear	Ba,Fe,B,b,C
A711	1.5	1450	360	IW	Clear	Ba,Fe,B,b,C
A813	2	1400	30	IW	Clear	Ba,Si,B
B339	0.7	1400	30	IWC	Clear	Ba,C,B,b
B341	0.7	1400	30	IWC	Clear	Ba,C,B,b
A808	1.5	1400	30	IWC	Clear	Ba,C,B,b
A811	2	1400	30	IWC	Clear	Ba,C,B,b
A809	3	1400	30	IWC	Clear	Ba,C,B,b
B338	1.5	1400	30	MMC	Clear	Ba,C,B,b
B340	1.5	*1400*	30	NNO	Clear	Si, B,b,C
Series 2 Andesite + O–H						
B386	1	1400	30	IW	Milky	
A882	1	1400	30	IW	Black	P
B403	1	1400	30	IW	Clear	P
A937	1.5	1400	30	IW	Clear	b
B430	2	1400	30	IW	Clear	B,b
A950	2	1500	10	IW	Black	B,b
B436	2.5	1400	2	IW	Clear	B,b
A953	2.5	1400	10	IW	Clear	B,b
A930	2.5	1400	30	IW	Clear	B,b
B423	2.5	1400	30	IW	Clear	P,B,b
A949	2.5	1500	10	IW	Clear	
A901	2.6	1400	30	IW	Clear	P,B
A936	3	1400	30	IW	Clear	B
B447	1.5	1400	30	MMC	Clear	P,B,b
B449	2	1400	30	MMC	Clear	P,B,b
B446	2.5	1400	30	MMC	Clear	B,b
B448	3	1400	30	MMC	Clear	P

[a] Notes: Ba= $BaCO_3$ sleeve used in piston cylinder assembly. All others used CaF_2. Fe, Fe outer capsule; P=Pressurized Quench; Si, metallic Si present; C, graphite present. Si inserted in inner capsule. B, large equilibrium bubbles in glass; b, small quench bubbles in glass.

[b] Buffer assemblages in outer capsule ($+H_2O$): IW, Fe+FeO; IWC, Fe+FeO+Fe_3C; MMC, Mo+MoO_2+Mo_2C; NNO, Ni+NiO.

Dissolved H_2, OH^-, and H_2O concentrations were measured by FTIR and for the basalt+COH series, total H concentrations by SIMS.

2.1. Starting materials

The synthetic basalt starting material (Supplementary data) included reduced C–O–H volatile components. In some cases graphite or Si metal was included in the inner capsules to influence C activity or f_{O2} (Table 1), but these did not affect the imposed f_{H2}. The andesite (Supplementary data) starting material was nominally C-free. The original intention for the first set of experiments was to study the solubility of methane, and results pertaining to C solubility will be presented elsewhere. The starting material for the basalt+COH experiments was prepared from albite, wollastonite, SiO_2, Al_2O_3, MgO, tetrakis-silane ($Si_5C_{12}H_{36}$), $Mg(OH)_2$ and $Al(OH)_3$ and H_2O. Those for the andesites were constructed from SiO_2, Al_2O_3 and synthetic minerals and glasses ($CaSiO_3$, $NaAlSi_3O_8$, $KAlSiO_4$) and H_2O (Supplementary data).

2.2. Experimental methods

All experiments were conducted in an end-loaded piston cylinder apparatus using assemblies consisting of crushable MgO, a graphite furnace and either $BaCO_3$ or CaF_2 salt sleeves (Table 1). For $BaCO_3$, a −0.2 GPa friction correction was applied (Xirouchakis et al., 2001), whereas the CaF_2 sleeves were employed without friction correction. CaF_2 produces a greater

initial quench rate than $BaCO_3$ (150 °C/s versus 100 °C/s). Other details of the experimental setup and calibration are given in Xirouchakis et al. (2001).

Experiments were conducted for times ranging from 2 min to 6 h. For the andesitic experiments, a time series from 2 to 30 min at 1400 °C and 2.5 GPa demonstrated H_2 concentrations in the inner capsule rapidly approach steady state (Table 2). In some experiments, a pressurization technique was employed to inhibit exsolution of vapor during quench (Table 1). This entailed raising the sample pressure by ~0.5 GPa coincident with termination of power to the furnace.

2.3. Buffering f_{H2}

To impose a known hydrogen fugacity, f_{H2}, on the samples, a double capsule technique (Eugster and Wones, 1962) was employed. An inner 2 mm diameter Pt capsule containing the sample was itself sealed in a 4 mm Pt capsule with an assemblage of crystalline phases plus fluid that fixes f_{H2}. Rapid diffusion of H through the Pt thereby imposed the same hydrogen fugacity on the melt in the inner capsule. Following the experiments, the persistence of buffering solids and fluid in the outer capsule were verified by optical inspection and Raman spectroscopy.

Several buffering assemblages in the outer capsule were used to fix f_{H2}:

$$\underset{\text{metal}}{Fe} + \underset{\text{oxide}}{FeO} + \underset{\text{fluid}}{H_2O} \quad (1a)$$

Table 2
Experimentally determined H_2 and H_2O concentrations.

Experiment	FTIR H_2 (wt.%)	FTIR H_2O[a] (wt.%)	SIMS H[b] wt.%	f_{H2} (bar)	ln K[c]
Series 1 Basalt + C–O–H					
B343	0.12	0.66	0.14(3)	5319	−11.94
A812	0.36	1.28	0.39(4)	19,557	−12.20
B337	0.30	1.25	0.33(6)	19,557	−12.37
A697	0.18	0.73	0.19(6)	19,058	−12.84
A711	0.26	0.52	0.13(1)	19,058	−12.47
A813	0.46	1.95	0.6(1)	36,491	−12.62
B339	0.07	1.94	0.44(8)	3492	−12.10
B341	0.09	1.71	0.45(2)	3492	−11.78
A808	0.18	1.57	0.48(2)	12,533	−12.43
A811	0.15	2.02	0.53(11)	23,338	−13.19
A809	0.28	2.59	0.8(1)	68,163	−13.71
B338	0.09	1.82	0.42(12)	11,148	−12.95
B340	n.d.	0.66	0.20(1)	166	−11.94
Series 2 Andesite + O–H					
B386	0.35	4.55		9285	−11.44
A882	0.11	2.29		9285	−12.63
B403	0.34	2.36		9285	−11.43
A937	0.64	3.35		19,562	−11.62
B430	0.80	4.10		36,478	−12.10
A950	0.20	2.45		39,066	−13.36
B436	0.86	2.56		63,206	−12.58
A953	0.86	4.66		63,206	−12.58
A930	0.87	4.75		63,206	−12.59
B423	0.90	4.68		63,206	−12.55
A949	0.93	6.91		67,129	−12.62
A901	0.90	4.77		72,269	−12.68
A936	0.90	5.74		104,109	−13.08
B447	0.40	3.05		11,115	−11.50
B449	0.56	3.44		20,365	−11.83
B446	0.66	3.84		34,867	−12.24
B448	0.67	6.35		56,987	−12.71

[a] Sum of observed H_2O and OH-, calculated as H_2O.
[b] Total hydrogen, including H_2O, OH–, molecular H_2, and CH_4 (H in $CH_4 < 0.01$ wt.% in all samples, Ardia et al. unpub. data).
[c] $K = X_{H2}/f_{H2}$, where X_{H2} is the mole fraction of H_2 in the melt, calculated on the basis of oxide components (including H_2O) and f_{H2} is the H_2 fugacity.

$$\underset{\text{metal}}{Ni} + \underset{\text{oxide}}{NiO} + \underset{\text{fluid}}{H_2O} \quad (2a)$$

$$\underset{\text{alloy}}{Fe} + \underset{\text{oxide}}{FeO} + \underset{\text{carbide}}{Fe_3C} + \underset{\text{fluid}}{H_2O} \quad (3a)$$

$$\underset{\text{metal}}{Mo} + \underset{\text{oxide}}{MoO_2} + \underset{\text{carbide}}{Mo_2C} + \underset{\text{fluid}}{H_2O} \quad (4a)$$

These assemblages fix f_{H2} in the outer capsule according to the following reactions:

$$\underset{\text{metal}}{Fe} + \underset{\text{fluid}}{H_2O} \Leftrightarrow \underset{\text{oxide}}{FeO} + \underset{\text{fluid}}{H_2} \quad (1b, 3b)$$

$$\underset{\text{metal}}{Ni} + \underset{\text{fluid}}{H_2O} \Leftrightarrow \underset{\text{oxide}}{NiO} + \underset{\text{fluid}}{H_2} \quad (2b)$$

$$\underset{\text{metal}}{Mo} + 2\underset{\text{fluid}}{H_2O} \Leftrightarrow \underset{\text{oxide}}{MoO_2} + 2\underset{\text{fluid}}{H_2} \quad (4b)$$

In assemblages (3) and (4), the imposed value of f_{H2} are modified by speciation of C–O–H fluids, which require evaluation of the activities of C imposed by the reactions

$$3\underset{\text{metal}}{Fe} + C \Leftrightarrow \underset{\text{carbide}}{Fe_3C} \quad (3c)$$

$$2\underset{\text{metal}}{Mo} + C \Leftrightarrow \underset{\text{carbide}}{Mo_2C} \quad (4c)$$

Sources of requisite thermodynamic data for the solid buffering phases are summarized in Table 3. C–O–H fluid fugacities in the outer capsules are calculated with the equation of state of Zhang and Duan (2009).

2.4. Analytical methods

Concentrations of H_2, OH, and H_2O in quenched glasses in both experimental series were quantified by FTIR using a Bruker Tensor 37 FTIR spectrometer and Hyperion 2000 microscope operated in transmission mode. Spectra were recorded over a range of 600–7500 cm^{-1}, averaging 256 scans, with a spectral sample spacing of 4 cm^{-1} in the frequency domain. A KBr beamsplitter was utilized with a mid-IR source, an unpolarized beam, and a square 100 × 100 μm spot. Molecular H_2 concentrations were quantified from the absorption peak near 4130 cm^{-1} (Fig. 1) using the integrated absorption coefficient determined from SiO_2 glass by Shelby (1994), as calibrations for aluminosilicate glasses are not available. The heights of the H_2 peaks were measured after subtracting cubic spline type baselines that follow the broader OH absorption band with which the H_2 peak is convoluted. The molecular bond of homonuclear H_2 vapor is not IR active, but the electric field gradient of the surrounding silicate matrix affects the symmetry of the H–H bond, resulting in weak infrared absorption of H_2 in silicate glasses. Consequently, small absorptions correspond to comparatively large concentrations. Concentrations of OH and H_2O were determined from the areas of the combination bands at 4500 and 5200 cm^{-1}, respectively, using integral molar absorption coefficients for andesitic glass from Ohlhorst et al. (2001). For each spectrum, the baseline used for the 4500 and 5200 cm^{-1} peaks was a convolution of a tangent to the minima surrounding the 5200 cm^{-1} peak and a Gaussian to fit the high frequency side of the 4000 cm^{-1} band (the 'GG' type baseline of Withers and Behrens, 1999). Sample thicknesses were determined by averaging 6–10 measurements made using a digital micrometer that has an accuracy of 0.01 mm. Uncertainty in sample thickness does not exceed 1%. The density of an anhydrous glass with major element composition based on microprobe analysis of the andesitic glass was calculated using the method of Fluegel (2007). The weight proportions of OH^- and H_2O and densities of the andesitic glasses were calculated assuming a linear decrease in glass density of 18.4 g/l for every

Table 3
Thermodynamic data and sources for calculation of experimental hydrogen fugacities (f_{H2}).

Free energy of Reactions at 1 bar/100 kPa:

Reaction	*Source*
$Fe+0.5O_2 = FeO$:	O'Neill (1988)
$Ni+0.5O_2 = NiO$[a]	Campbell et al. (2009)
$Mo+O_2 = MoO_2$	Bygden et al. (1994)
$3Fe+C = Fe_3C$	Hallstedt et al. (2010)
$2Mo+C = Mo_2C$	Iwai et al. (1986)

Equation of state data for extrapolating free energies to high pressure: molar volume (V_0), bulk modulus (K) and thermal expansivity (α)

Phase	V_0 (J/GPa)	K (GPa)	dK/dP	α (X10^5)
Fe	7076[b]	133[b]	5[b]	7.7[c]
$Fe_{1-x}O$	12,256[b]	146.9[b]	4[b]	4.2[b]
Mo	9376[d]	232[d]	3.82[d]	2[d]
MoO_2	19,770[e]	160[e]	5[e]	3[f]
Fe_3C	23,190[g]	199[h]	10[h]	4.18[g]
Mo_2C	22,369[i]	307[j]	6.2[j]	2.3[i]
C	5286[k]	33.8[l]	8.9[l]	4.15[k]

[a] Calculation of Ni–NiO reaction at high pressure is taken directly from Campbell et al. (2009).
[b] Campbell et al. (2009).
[c] Wood (1993).
[d] Zhao et al. (2000).
[e] Fried et al. (2002).
[f] Estimated.
[g] Wood et al. (2004).
[h] Duman et al. (2004).
[i] Epicier et al. (1988).
[j] Haines et al. (2001).
[k] Lowitzer et al. (2006).
[l] Hanfland et al. (1989).

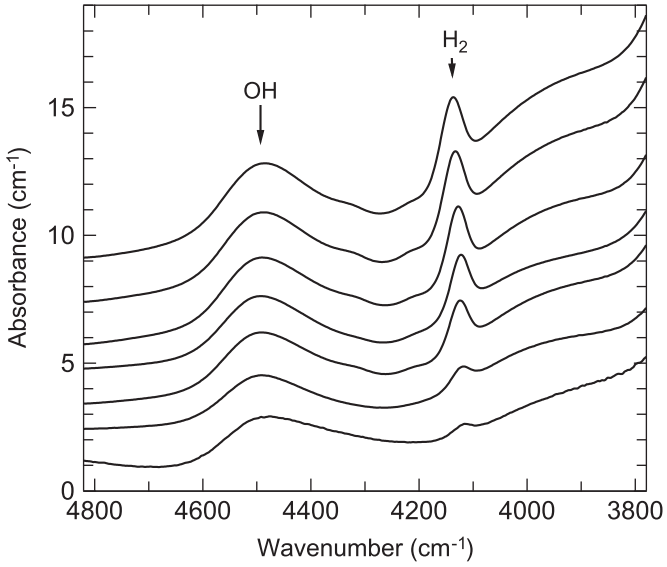

Fig. 1. FTIR spectrum of selected glasses, showing the well-resolved molecular H_2 absorption peak near 4130 cm^{-1}. From top to bottom, spectra are from experiments A901, A953, B430, A937, B449, A950, and A882.

wt.% increase in c_{water}, where c_{water} is the sum of OH and H_2O species concentrations expressed as wt.% H_2O (Ohlhorst et al., 2001). For the basalt+COH glasses, spectra were recorded 5 days before SIMS analyses and again 3 months afterwards. No differences in concentrations were found, suggesting that H_2 loss was not appreciable over the ~4 months elapsed between the experiments and the final FTIR analyses. Andesite glasses were stored at −2 °C between experiments and analyses and repeat analyses 2 months apart produced identical results.

Major element compositions of selected quenched glasses (Supplementary data) were determined by EMPA using a JEOL JXA8900R using a 15 kV acceleration voltage, 10 nA beam current, and a partially defocused beam (5 μm). Count times were 20 s for the peak and 10 s for the background for all elements except Na and K, which were always counted first on their respective spectrometers for 10 s and 5 s. Natural mineral and glass standards were used for calibration.

SIMS analyses of H in the basaltic glasses were conducted using the CAMECA 6f at Arizona State University, using a primary Cs^+ ion source, counting negative $^{16}OH^-$ ions, employing methods and standards described in detail in Tenner et al. (2009). SIMS measures total H content of the glass, which includes H_2, OH^- and H_2O species. Subtraction of the OH– and H_2O concentrations measured by FTIR (Table 2) yields an estimate of the molecular H_2 content and this can be compared to that measured directly by FTIR.

3. Results

3.1. Textures

After some trial and error, experiments were produced with large areas of clear bubble-free glass. However, vapor bubbles were common features (Table 1), including large (from 50 μm to several 100 μm) ones inferred to represent saturation with a fluid during the experiment and regions with many finely dispersed smaller (<20 μm and commonly <5 μm) bubbles believed to have formed during quench. FTIR analyses were performed on glass chips free of observable bubbles. Because H_2 vapor is not IR-active, incidental vapor bubbles that might have been sampled by the infrared beam did not contribute to the observed IR absorption near 4130 cm^{-1}, which we attribute entirely to H_2 dissolved in silicate.

In some glasses from the basalt+COH series, precipitates of carbon nanofibers were common (Table 1). Areas free of precipitates were found for FTIR analysis. One glass from the andesite series (B386) appeared milky, perhaps from very fine exsolved fluids, but the measured H_2 concentration was the within error of

that measured in a repeat experiment (B403) that produced clear glass. In two experiments from the andesite series, A882 and A950, glasses appeared black owing to precipitation of a finely dispersed carbon phase. The carbon in these nominally carbon-free experiments may have been introduced during poorly administered capsule welds. These had anomalously low H_2 concentrations compared to other experiments at similar conditions. We surmise that carbon precipitation interfered with these charges, either by catalyzing H_2 exsolution on quench or by inhibiting preparation of glass chips with adequate optical transmission. These two samples were not used for thermodynamic calibration.

3.2. FTIR and SIMS observations of dissolved O–H components

We used the IR absorption near 4130 cm^{-1} to quantify molecular H_2 concentrations (Fig. 1). The observed peak centroid in the quenched glasses varied from 4105 to 4140 cm^{-1} and increased with experimental pressure along a trend similar to that observed in Raman spectra of Na_2O–Al_2O_3–SiO_2 glasses (Luth et al., 1987,Fig. 2). As noted by Luth et al. (1987), the trend for molecular H_2 dissolved in glass is about 50 wavenumbers below that for gaseous hydrogen. Concentrations of dissolved molecular H_2 measured by FTIR in the basaltic starting materials range from below limit of detection up to 0.46 wt.%, whilst those for andesite are higher, ranging from 0.11 to 0.93 wt.% (Table 2). Ranges of concentrations of H_2O, based on IR measurements of OH^- and H_2O, are 0.52–3.52 and 2.45–6.91 wt.%, in the basaltic and andesitic series, respectively. We find no evidence in the FTIR spectra for Si–H complexes, which would be expected near 2250 cm^{-1} (e.g., Schmidt, 1998). Concentrations of total H measured by SIMS, measured only for the basaltic series, range from 0.14 to 0.8 wt.% (Table 2).

Concentrations of molecular H_2 measured by FTIR and those estimated by the combination of SIMS H measurements and OH^- and H_2O quantified by FTIR are of the same magnitude, with no systematic bias to greater or lesser concentrations depending on method, but comparison of individual measurements show considerable scatter (Fig. 3). Analyses of molecular H_2 concentrations by FTIR have good precision, as the H_2 peaks are well-resolved

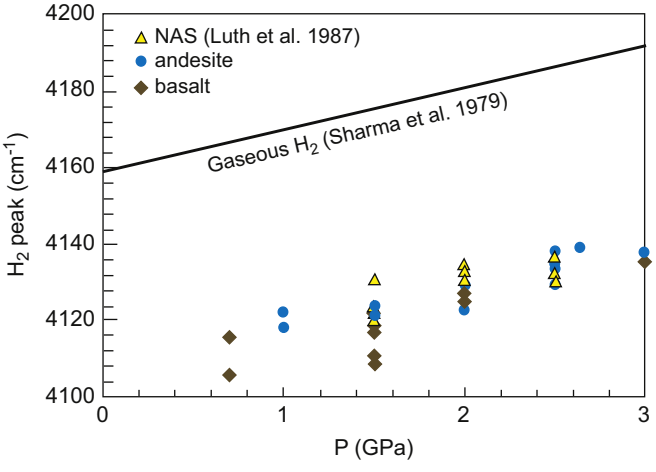

Fig. 2. The centroid of the IR peak attributed to molecular H_2 in glasses increases with the pressure of quench. In addition to the basaltic and andesitic glasses from the present study, the plot includes Raman observations of NAS (Na_2O–Al_2O_3–SiO_2) glasses from Luth et al. (1987). The observed trend is parallel to that for H_2 vapor (Sharma et al. 1979), but displaced lower by about 50 wavenumbers. This supports the interpretation that the observed absorption is owing to molecular H_2 chemically dissolved in glass, rather than present as vapor in microbubbles (which in any case, is not IR active).

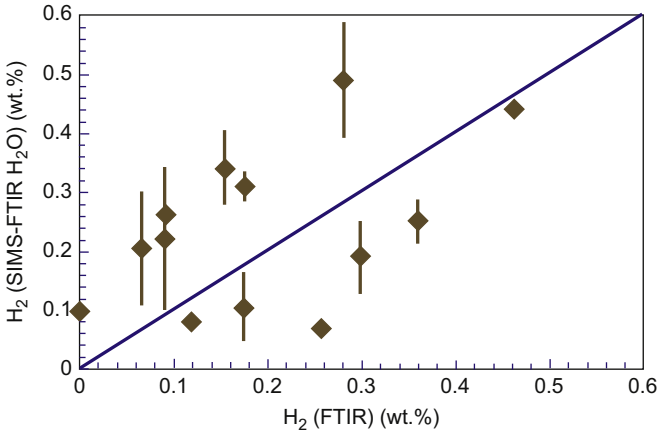

Fig. 3. Comparison between molecular H_2 determined directly by FTIR with that estimated by subtracting H_2O and OH^- determined by FTIR from the total H measured by SIMS for the basalt+COH series Error bars for determinations by SIMS-FTIR (H_2O+OH^-) include only the uncertainty on the SIMS measurements. The scatter in this plot reflects the propagated error in the precision of the H_2 measurements by subtraction of FTIR from SIMS, but the similar magnitude of the values between the two methods supports the overall accuracy of both methods.

from background (Fig. 1), but because they are derived with an absorption coefficient calibrated from SiO_2 rather than natural mafic glass, their accuracy is subject to considerable uncertainty, possibly more than 100%. On the other hand, the concentrations determined by subtracting FTIR-determined OH and H_2O from SIMS measurements of H have much better accuracy, but low precision owing to the effects of propagation of errors in subtraction. Thus, the scatter in Fig. 3 is owing chiefly to low precision of the H_2 derived from the SIMS data. The similar magnitude of the two determinations of molecular H_2 strongly suggests that the accuracy of the FTIR-determined molecular H_2 concentrations is reasonably good, with an uncertainty of perhaps $\pm 50\%$. Calibration of IR absorption coefficients for natural glasses is needed.

4. Thermodynamic treatment

Hydrogen solubility in silicate liquids is controlled by the reaction:

$$H_{2\,vapor} \Leftrightarrow H_{2\,magma} \tag{5}$$

and the equilibrium constant

$$\ln K = \ln \frac{X_{H2}^{magma}}{f_{H2}} = \ln K_0 + \frac{\Delta H}{R}\left(\frac{1}{T_0} - \frac{1}{T}\right) - \frac{\Delta V(P-P_0)}{RT} \tag{6}$$

where X_{H2}^{magma} is the mole fraction of dissolved H_2, ΔH and ΔV are the enthalpy and volume of the reaction, respectively, and K_0 is the value of the equilibrium constant at the reference temperature and pressure (T_0=1400 °C, P_0=100 kPa). The spread of temperatures in our experiments does not permit calibration of ΔH, but variations of ln K versus pressure suggest, for basalt and andesite, ln K_0= −11.4 and −10.6 and ΔV= 10.6 and 11.3 cm^3/mole, respectively (Fig. 4).

5. Discussion

5.1. Comparison to previous work and effects of composition on solubility of molecular H_2.

Observed solubilities of molecular H_2 are similar to those found previously for obsidian (Gaillard et al., 2003) and silica

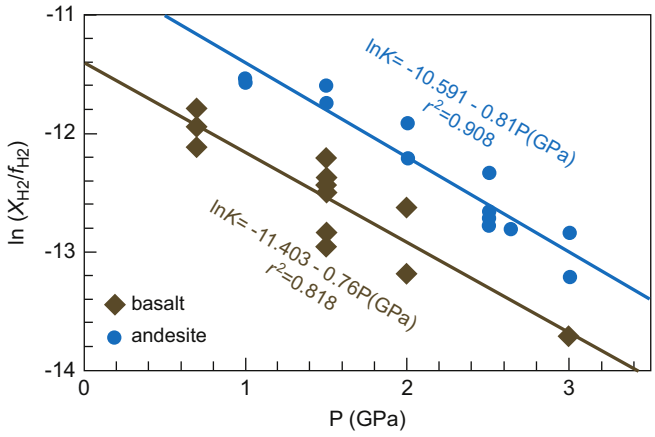

Fig. 4. Calculated equilibrium constant $K = X_{H2}/f_{H2}$ (Eq. (6)) for basalt and andesite series experiments versus pressure. Values of X_{H2}, the mole fraction of molecular H_2 in melts, were calculated from the melt compositions (Supplementary data) based on oxide components including H_2O. Hydrogen fugacities, f_{H2}, were calculated from the equation of state of Zhang and Duan (2009). Linear regression of each trend yields values for $\ln K_0$ (−11.4 for basalt, −10.6 for andesite) in Eq. (6), whereas the slopes (−0.76/GPa and −0.81/GPa) yield values of the partial molar volume of H_2 of 10.6 and 11.3 cm^3/mole, respectively.

glass (Schmidt, 1998), which yield values of $\ln K_0$ (−11.4 and −11.5, respectively) nearly identical to that which we determine for basalt+COH. However, comparison to these data may not be straightforward, as they derive from very different compositions, temperatures (<950 °C), pressures (0.2 GPa, Schmidt, 1998; 0.007 GPa, Gaillard et al., 2003) and experimental techniques.

The greater solubility in the andesite melt compared to basalt may be owing to difference in ionic porosity (IP), as has been observed for other neutral molecules such as noble gases, CO_2, and N_2 and this has been attributed to a corresponding increase in ionic porosity (IP) (Carroll and Stolper, 1993). Ionic porosity is an estimate of the volume of silicate melt, V_m, that is not occupied by the ions, V_i, and was calculated as $100*(1-V_i)/V_m$, following Carroll and Stolper (1993), using the ionic radii of Shannon (1976) (except for H in H_2O, which was taken from Nuccio and Paonita (2000)), with V_m calculated at 1400 °C and 1.5 GPa by application of the pMELTS model (Ghiorso et al., 2002). The calculated IP for the melts in this study are near 45.6 and 48.3 for basalt and andesite, respectively (Supplementary data). We note that this explanation would predict much higher solubilities than have been observed for obsidian (Gaillard et al., 2003) and SiO_2 glass (Schmidt, 1998), but data at comparable temperatures, pressures, and experimental techniques are required before this comparison can be given much weight.

Correlation between H_2 solubility and IP, although tenuously based on just two observations, allows for the possibility of extrapolation to other melt compositions. The difference in $\ln K_0$ between basalt and andesite amounts to ~0.3 per unit of ionic porosity. Carroll and Stolper (1993) found that the influence of melt ionic porosity on the solubility of noble gases is proportional to atomic radius: e.g., $\ln K_0$ increases by 0.34 per unit of IP for He, 0.68 for Ne and so on. The value for molecular H_2 is in accord with its mean molecular radius similar to He. Extrapolation of the andesite and basalt solubility laws to a melt with the ionic porosity of peridotite (IP=42.1) give an $\ln K_0$ of −12.5. This suggests that at a given pressure and oxygen fugacity, the solubility of H_2 in magma oceans is markedly less than observed in basalt. If our correlation of solubility with IP is spurious, then employing this low value of $\ln K_0$ will give minimum estimates of solubility.

An alternative explanation for the difference in H_2 concentrations between the two experimental series is that it is owing to the effects of C on H_2 solubility. This interpretation would be consistent with the observations of the two black andesitic glasses that were contaminated with carbon and have apparent H concentrations comparable to those from the basaltic series (Table 2). Still, this explanation seems to us unlikely. Any effect of C on H_2 solubility would be owing to the influence of the C dissolved in the melt, and the concentrations in the basaltic melts are very small (<500 ppm; <0.2 mole% CH_4, Ardia et al., unpublished data). Also, the effect, if any, should be proportional to the dissolved CH_4 concentrations, which increase with pressure by more than a factor of 5 in the basaltic glasses, which seems inconsistent with the systematic offset between the two experimental series as well as their similar dependence on pressure (Fig. 4).

5.2. Calculated solubilities as a function of pressure and oxygen fugacity

Application of the solubility laws derived in Section 4 allows calculation of the solubility of molecular hydrogen as a function of pressure (Fig. 5). For basalt coexisting with pure hydrogen, solubility increases with pressure to about 0.57 wt.% at 1 GPa. On a molar basis, this is equivalent to 5 wt.% H_2O solubility. Calculated solubilities for melts of peridotitic composition, extrapolated based on the diminished ionic porosity of ultramafic liquids, are smaller than for basalt by about a factor of 3 (Fig. 5), such that at 1 GPa in the presence of pure H_2, the molecular H_2 concentration is 0.19 wt.%.

It is also possible to calculate solubility as a function of pressure at fixed f_{O2} relative to standard buffers by calculating f_{H2} for O–H fluids (Fig. 5). For conditions typical of magmatism in Earth's shallow mantle and crust (>IW+3 e.g., Frost and McCammon, 2008), molecular H_2 concentrations are small (<76 ppm at 1 GPa) and become more significant under reducing conditions, reaching 4700 ppm at IW-2 and 1 GPa (Fig. 5).

Combination of the new H_2 solubility law with one for H_2O (Moore et al., 1998) allows calculation of the concentrations of dissolved H_2 and H_2O in basalt-OH system as a function of pressure and oxygen fugacity. The proportion of molecular H_2 increases as conditions become more reducing, but is also quite sensitive to both pressure and total bulk H content. This

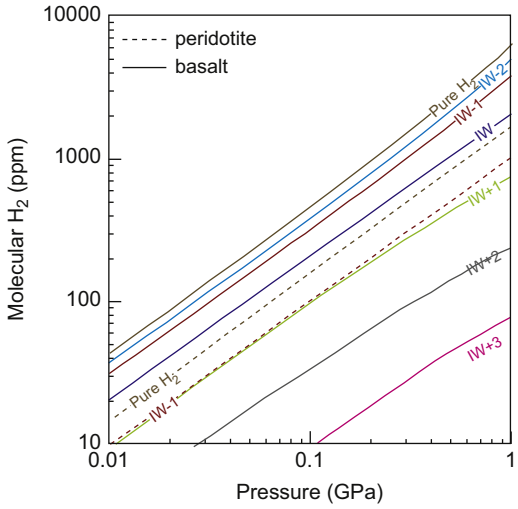

Fig. 5. Solubility of H_2 in basaltic magma calculated for melt coexisting with pure H_2 and with O–H vapor at oxygen fugacities fixed between 2 log units below IW and 3 log units above. Also shown is the calculated solubility for peridotitic liquid in the presence of pure H_2 and for IW-1, based on the assumption that this can be predicted from the ionic porosity of silicate liquids. Hydrogen fugacities are calculated from the equation of state of Zhang and Duan (2009).

is because H_2 solubility increases with f_{H2} (Eq. (2)), whereas H_2O solubility increases with the square root of f_{H2O} (e.g., Moore et al., 1998). At given oxygen fugacity relative to IW, magmatic H_2O (or OH−) dominates in dry magmas at low pressure and H_2 becomes increasingly important in high pressure H-rich bulk compositions (Fig. 6A). Thus, at low pressure (0.1 GPa) and low total H contents (100 ppm H, equivalent to 0.09 wt.% H_2O), $H_2/(H_2+H_2O)$ is not more than 10% even at conditions as reducing as IW-2. But at 3 GPa and modest H contents (1700 ppm H, equivalent to 1.5 wt.% H_2O), 18% of the total H will be H_2 at IW and 50% will be at IW-2. Therefore, molecular H_2 is not a significant volatile species for dry magmas at near-surface conditions, such as those from the Moon, but may be more important for more hydrous compositions at mantle pressures. For example, for typical sources (~1 GPa) of the most reduced Martian basalts at IW-0.7 (Wadhwa, 2008) and bulk H contents of 500–1000 ppm (McCubbin et al., 2010a), > 10 % of the H will be molecular H_2. At higher pressures associated with deep partial melts in the Earth or with core formation, molecular hydrogen can potentially become dominant.

Additionally, the pressure dependence of $H_2/(H_2+H_2O)$ may contribute to a vertical redox gradient in a magma column, as the $H_2/(H_2+H_2O)$ fixed by equilibration at high pressure corresponds to even more reduced conditions at low pressure (Fig. 6B). Dissolved H_2 and H_2O form a redox couple according to the reaction:

$$\underset{\text{magma}}{H_2} + \frac{1}{2}O_2 \Leftrightarrow \underset{\text{magma}}{H_2O} \quad (7)$$

The pressure and f_{O2} dependence of this reaction can produce redox change with depth in a column of magma, either in a magma ocean or in a basalt ascending from its source. In the absence of other redox reactions, a magma with a given $H_2/(H_2+H_2O)$ ratio would, upon decompression, become more reduced (Fig. 6B). In fact, other redox couples in natural magmas, such as those between oxidized and reduced forms of iron or carbon, also have pressure dependences (e.g., Hirschmann, 2012) and the overall polybaric redox evolution will be a product of the interactions between these. For example, the Fe metal globules in lunar basalts (e.g., Weitz et al., 1997) could conceivably be precipitated owing to a reaction such as $H_2 + FeO = Fe + H_2O$ though, based on the discussion in Section 5.6 below, it is not clear if there was sufficient H_2 in lunar magmas to account for the quantity of observed metal.

5.3. Dissolution of the nebular atmosphere into a molten earth

The solar nebula persisted for the first ~10 Ma (Greaves, 2005) of solar system history, during which time Earth grew to ~25–40% of its ultimate mass (Raymond et al., 2009) amid an atmosphere consisting chiefly of H_2. High temperatures associated with impacts, core formation, and to a lesser extent, radioactive decay make it likely that a magma ocean was present for at least part of this early era of planetary growth and differentiation, and so some of the primordial atmosphere inevitably was absorbed by the growing rocky planet. Previously it has been thought that the H dissolved in the magma ocean would be in the form of H_2O, generated by reactions such as

$$\underset{\text{vapor}}{H_2} + \underset{\text{melt}}{FeO} \Leftrightarrow \underset{\text{alloy}}{Fe} + \underset{\text{melt}}{H_2O} \quad (8)$$

(e.g., Kuramoto and Matsui, 1996) and it has been argued that this could be the source of significant fraction of the inventory of H_2O now residing in Earth's mantle and oceans (Ikoma and Genda, 2006; Genda and Ikoma, 2008). Although reactions such as this may have occurred, much of the nebular H partitioned into the growing solid Earth instead could have dissolved as molecular H_2.

The amount and fate of nebular hydrogen absorbed by an early magma ocean depend on a number of factors, including the magma mass, the availability of metal and the atmospheric pressure. This pressure is determined by the gravitational acceleration imposed by the growing protoplanet (50–70% of present-day gravity if the mean planet density is similar to that of Earth) and, more critically, on the mass of the atmosphere. Unfortunately, this last quantity is not well constrained, but could be in the range of 10^{20}–10^{22} kg (Ikoma and Genda, 2006). For a protoplanet 25–40% of the mass of the present Earth, this would generate between 10 and 1500 bar H_2 pressure, which in turn could dissolve between 1 and 220 ppm H_2 in an underlyng peridotitic magma ocean. Though the low end of this range signifies negligible storage in the interior, the high end amounts to about 2 "oceans" of hydrogen in a mantle 40% of its modern mass. Much of this hydrogen in turn would partition into available metal and be delivered to the core. Assuming that loss of H_2 to the core leads to further solution of the atmosphere into the magma, even the modest solubilities could ultimately deliver a substantial mass of nebular hydrogen to the core. Because the H_2 dissolved in this way is then hidden in the core, the amount of nebular H in Earth's interior is not constrained either by the D/H

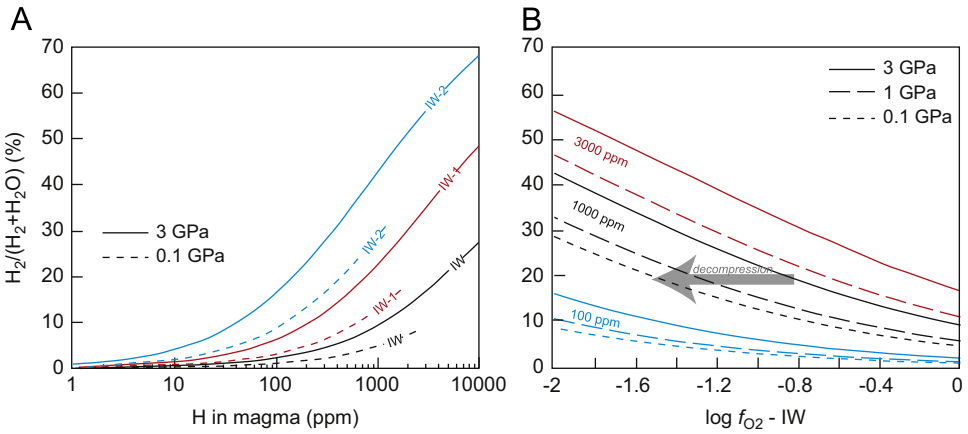

Fig. 6. Calculated molar ratio H_2/H_2+H_2O as a function of f_{O2}, pressure, and bulk H (H_2+H_2O) content of the magma. Hydrogen solubilities are calculated as in Fig. 5, and H_2O solubility calculated from Moore et al. (1998). (A) At a given f_{O2} and relative to IW and pressure, $H_2/(H_2+H_2O)$ increases with increasing bulk H concentration, as the high intrinsic solubility of H_2O is partly overcome by increases in H_2 fugacity because the solubility of H_2 increases linearly with f_{H2} whereas that for H_2O with the square of f_{H2O}. Low pressure curves terminate when concentrations reach vapor saturation. (B) At a given bulk H concentration and pressure, $H_2/(H_2+H_2O)$ ratio increases with decreasing f_{O2}. Note that for a magma with a given $H_2/(H_2+H_2O)$ ratio, decompression leads to a decrease in f_{O2}. There is no curve for 3000 ppm H at 0.1 GPa because such concentrations are oversaturated (i.e., see A).

ratio or the inventory of noble gases in the mantle today, as these may have been overprinted by subsequent additions and losses.

5.4. Hydrogen exchange between melt and core-forming alloy

Experimental studies of reaction between hydrous silicate melts and iron demonstrate the stability of iron hydride species, resulting in significant partitioning of H into core-forming alloy (Stevenson, 1977; Fukai, 1984; Okuchi, 1997; Ohtani et al., 2005). This reaction has been widely interpreted to be tied to oxidation of the magma (e.g., Drake, 2005; Ohtani et al., 2005; Bond et al., 2010; Rubie et al., 2011), with dissolved H_2O disproportionating to form H dissolved in the hydride and excess O remaining in the melt:

$$\left(1+\frac{x}{2}\right)\underset{\text{alloy}}{\text{Fe}}+\frac{x}{2}\underset{\text{melt}}{H_2O}\Leftrightarrow\underset{\text{alloy}}{FeH_x}+\frac{x}{2}\underset{\text{melt}}{FeO} \quad (9)$$

If applicable, reaction (9) limits the mass of hydrogen in the core to no more than 0.55 wt.%, or the equivalent of 50 "oceans", as the associated FeO produced could not exceed the 8 wt.% present in the mantle today. Although this upper limit is quite generous, it is less than some of the more extreme estimates of core H content (Okuchi, 1997; Williams and Hemley, 2001).

In fact, magma-metal equilibration associated with core formation occurred at very high mean pressures (>25 GPa, e.g. Li and Agee, 1996; Corgne et al., 2008). As seen by extrapolation of the curves in Fig. 6B to higher pressure, these are conditions at which most of the H present in melts in equilibrium with Fe metal (at IW-2 to IW-1) should be H_2, rather than H_2O. Consequently, reaction (9) is likely not an accurate portrayal of the process by which H enters the core. An additional key reaction is

$$2\underset{\text{alloy}}{\text{Fe}}+x\underset{\text{melt}}{H_2}\Leftrightarrow 2\underset{\text{alloy}}{FeH_x} \quad (10)$$

This reaction does not involve oxidation of Fe to FeO, and so solution of large amounts of H in the core need not be associated with oxidation.

One currently favored class of models for origin of the Earth's core considers that much of the process occurred under highly reducing conditions, thereby allowing significant Si to enter the core (Wood et al., 2006; Frost et al., 2008; Rubie et al., 2011). Rubie et al. (2011) considered these models to be inconsistent with sequestration of large amounts of H in the core, as the oxidizing effect of reaction (9) would eliminate the reducing conditions needed to stabilize Si. However, if H transport into the core is chiefly driven by reaction (10), then there may be no incompatibility between significant H and Si in early core-forming alloys.

In detail, the question of mantle oxidation by dissolution of H in core-forming alloy is a little more complicated. Although formation of Fe hydride via reaction (10) does not require oxidation of Fe to FeO by disproportionation of H_2O, there is an indirect effect. Because the magmatic $H_2/(H_2+H_2O)$ ratio depends on f_{O2}, loss of dissolved H_2 to coexisting alloy diminishes $H_2/(H_2+H_2O)$ in the melt, which tends to drive the magma toward oxidized conditions. Maintenance of equilibrium with Fe-metal resists this through the reaction:

$$\underset{\text{alloy}}{\text{Fe}}+\underset{\text{melt}}{H_2O}\Leftrightarrow\underset{\text{melt}}{FeO}+\underset{\text{melt}}{H_2} \quad (11)$$

Therefore, loss of H from magma to core will occur through an appropriate combination of reactions (9) and (10), such that the redox state evolves as FeO, H_2, and H_2O concentrations in the magma change. But because the $H_2/(H_2+H_2O)$ ratio required to maintain reducing conditions diminishes with H concentration in the magma (Fig. 6A), the amount of oxidation resulting will be small. Alternatively, if the magma is in contact with an H_2-rich atmosphere, the $H_2/(H_2+H_2O)$ ratio of the magma could be maintained by dissolution of additional H_2 vapor directly into the magma, without the formation of FeO. In this latter case, one may consider H transport from the atmosphere to the core via the mantle as a neutral process, without affecting the redox state of the mantle. Thus, hydrogen delivery to the core by direct dissolution of atmospheric H_2 in a magma ocean and subsequent reaction with core forming metal would be limited only by the mass of available hydrogen in the atmosphere present through the era of core formation. A nebular atmosphere of 10^{20}–10^{22} kg (Ikoma and Genda, 2006) amounts between 0.5 and 50 "oceans" of hydrogen and 0.005 and 0.5% of the ultimate mass of the core. Consequently, nebular H could be a significant portion of the H on Earth and a substantial minor component in the core without having left a marked geochemical imprint on the mantle.

5.5. Hydrogen in lunar basalts

Recent documentation of H in lunar glass beads, melt inclusions, and apatite crystals (Saal et al., 2008; Boyce et al., 2010; Greenwood et al., 2011; McCubbin et al., 2010a; Hauri et al., 2011) has generated considerable interest in the concentrations, significance, and origin of lunar "water". Lunar basalts are highly reduced, with oxygen fugacities similar to IW-1 $\pm$ 1 (Wadhwa, 2008), leading to the assertion that much of the H was present as molecular H_2 (Elkins-Tanton and Grove, 2011). However, the most hydrous lunar glasses yet identified have no more than 150 ppm H (Hauri et al., 2011) and this severely limit the proportion of H that may be H_2. For example, at IW-2 and 0.1 MPa, no more than 10% (15 ppm) of such magma will be molecular H_2 (Fig. 6B). In this melt's source region, ($\sim$0.5–2.5 GPa; Longhi, 1992), as much as 20% may be H_2. Based on apatite compositions, McCubbin et al. (2010a) estimated that late-crystallizing melts from an olivine gabbro (NWA 2977) had 800–1800 ppm H, of which, 20% would have been H_2 at IW-1 and 37% at IW-2.

Although a modest fraction of the H in lunar magmas may have been molecular hydrogen, there is little chance of directly sampling this H_2 today. Room temperature determinations of H_2 diffusivity in vitreous silica (Shang et al., 2009) suggest characteristic diffusion distances of $\sim$1 mm in 40 years, allowing escape of most of the molecular hydrogen present in lunar glass beads since their collection in 1969–1972. Diffusivity in basalt may be slower than in SiO_2 glass, but quantitative H_2 loss during the >3 GPa residence on the lunar surface is likely unavoidable.

The concentration and origin of lunar hydrous components are a matter of debate. Lunar mantle H estimates span a large range from 0.007–2 ppm (McCubbin et al., 2010a) up to 9–45 ppm (Hauri et al., 2011), and it is not yet established whether the bulk of this H was incorporated during formation of the Moon or added afterward (Greenwood et al., 2011; McCubbin et al., 2010a; Elkins-Tanton and Grove, 2011; Hauri et al., 2011). Juvenile H would presumably have been dissolved in the magma ocean, but the concentration incorporated in the lunar interior this way would have been proportional to the vapor pressure of an overlying H-rich atmosphere. The combined H_2 and H_2O solubility laws indicate that any such atmosphere must have been chiefly H_2 (90% if the average f_{O2} of the magma ocean was at IW-2, 74% at IW-1, or 48% at IW). Dissolution of 1 ppm total H in the magma at IW-1 would require 4 mbar atmospheric pressure, whereas for 10 and 50 ppm at IW-2 the atmosphere would have to amount to 0.55–8 bar, respectively (Fig. 7). As pointed out by Elkins-Tanton and Grove (2011), retention of appreciable juvenile H in the solidifying lunar magma ocean requires persistence of an atmosphere of this magnitude at least until the magma became sealed by its anorthosite carapace. Bulk mantle concentrations of

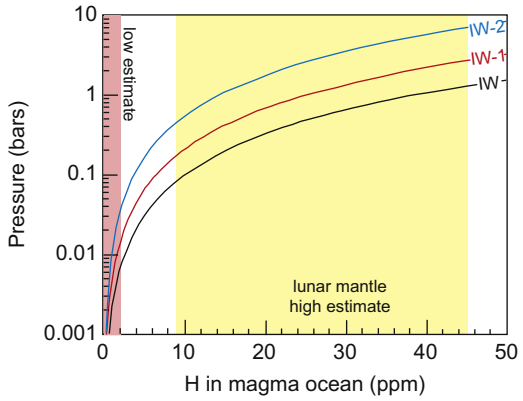

Fig. 7. Atmospheric pressure calculated above a lunar magma ocean with a given bulk H concentration for different oxygen fugacities in the coexisting magma and vapor. At IW-2, IW-1, and IW, the atmosphere consists of 90%, 74%, and 48% H_2, respectively. Atmospheric pressure is the sum of H_2O and H_2 partial pressures (and so neglects the partial pressure of any C-containing species). The high (9–45 ppm) and low (64 ppb–2 ppm) estimates for lunar mantle H concentration are from Hauri et al. (2011) and McCubbin et al. (2010a), respectively.

<2 ppm (e.g., McCubbin et al., 2010a) require only that a thin 10 mbar atmosphere survive until the magma ocean was isolated from the surface, but higher estimates of mantle concentrations (9–45 ppm, Hauri et al., 2011) require a thicker atmosphere of 100 mbar or greater (Fig. 7). Given high escape rates of H_2 from the low gravity environment of the Moon, retention of such a substantial atmosphere may be unlikely, in which case evidence for comparatively high lunar mantle H contents may point towards late delivery rather than juvenile sources (Greenwood et al., 2011; Elkins-Tanton and Grove, 2011).

5.6. Hydrogen in modern deep partial melts

In the modern deep Earth, hydrous partial melting may be widespread above the 410 km discontinuity (Bercovici and Karato, 2003; Tauzin et al., 2010) and in the shallow and deep portions of the lower mantle (Hirschmann, 2006). Quantitative extrapolations from experiments $\leq$ 3 GPa to the speciation of O–H fluids >13 GPa is unwise, but the qualitative trend evident in Fig. 6B indicates that at the IW buffer at 400 km, hydrogen could be the dominant hydrous species dissolved in mafic partial melts. At pressures of the lower mantle, the bias towards dissolved H_2 could be even stronger. We note however that the high pressure (>5 GPa) magmatic solubility of other neutral species such as noble gases are significantly lower than estimates extrapolated from low pressure data, owing to the collapse of ionic porosity in densified melts (e.g., Guillot and Sator, 2012), and so higher pressure experiments are needed.

The influence of volatiles on the melting relations of peridotite is modified when the volatile species change from oxidized to reduced. Reduced C–O–H volatiles have a smaller effect on the peridotite solidus than their oxidized ($H_2O \pm CO_2$) equivalents (Taylor and Green, 1988; Jakobsson and Holloway, 2008), perhaps owing to lower solubilities. At a given depth and temperature in the mantle, the concentrations of volatile components required to stabilize a partial melt may vary with oxygen fugacity. However, comparatively little is known about the melting relations of peridotite in the presence of reduced volatiles at pressures applicable to the deep upper mantle and beyond. For example, compositions of low-degree partial melts are unknown, as are the concentrations of different dissolved volatile species as a function of temperature or oxygen fugacity.

A key factor influencing the fate and distribution of deep volatile-rich partial melts is their buoyancy. A principle feature of the TZWF model of Bercovici and Karato (2003) is negative buoyancy of hydrous partial melts in the deepest part of the upper mantle, leading to ponding atop the transition zone. Experimental support for this hypothesis was provided by Matsukage et al. (2005) and Sakamaki et al. (2006), who found that the reduction in melt density effected by H_2O at high pressure is modest, and concluded that hydrous partial melts could be denser than surrounding mantle at 400 km. (Although Hirschmann et al., 2006 questioned whether partial melts with sufficient dissolved H_2O to be stable along the mantle geotherm would remain negatively buoyant.) Of course, the effect of dissolved H_2 on melt density will not be the same as for H_2O.

The thermodynamic calibration of H_2 solubilities (Fig. 4) yields a partial molar volume of dissolved H_2 of $\sim$11 cm^3/mole, which translates to an extremely low partial specific density (0.18 g/cm^3). This is dramatically smaller than the low pressure partial specific density of H_2O (0.65 g/cm^3, Ochs and Lange, 1999). Similar to H_2O, molecular H_2 is likely highly compressible in silicate melts, and so its influence on the density of high pressure magmas remains uncertain. What is clear is that H_2-rich magmas could have low density compared to H_2O-rich magmas with comparable total H contents and that inferences about the buoyancy of partial melts in the deep mantle based on the properties of H_2O in silicate liquids should be reexamined.

6. Conclusions

Molecular H_2 can be a significant hydrous species in silicate liquids under reducing conditions applicable to planetary and deep Earth magmas. It obeys a simple solubility law proportional to the hydrogen fugacity and pressure. Solubilities are systematically greater in andesite than in basalt, with the difference apparently related to variations in ionic porosity, and this suggests that solubilities in ultramafic liquids will be smaller than those in experimentally accessible melt compositions. Significant solubility of magmatic H_2 indicates that partitioning of hydrogen during early planetary differentiation was not necessarily linked to redox evolution. Lunar basalts, though highly reduced, likely have very low $H_2/(H_2+H_2O)$ ratios, owing to low total H contents. Because magmatic H_2 is stabilized by high pressure under reducing conditions, it may be the principal hydrous species in magmas in the deep Earth.

Acknowledgments

We thank Lynda Williams and Rick Hervig for assistance with SIMS measurements at ASU and Malcolm Rutherford and Huaiwei Ni for helpful reviews. We gratefully acknowledge funding from NASA (NNX11AH13G and NNX11AG64G) and from NSF (EAR0757903 and EAR1161023).

Appendix A. Supporting information

Supplementary data associated with this article can be found in the online version at http://dx.doi.org/10.1016/j.epsl.2012.06.031.

References

Bercovici, D., Karato, S., 2003. Whole-mantle convection and the transition-zone water filter. Nature 425, 39.
Bond, J.C., Lauretta, D.S., O'Brien, D.P., 2010. Making the Earth: Combining dynamics and chemistry in the solar system. Icarus 205, 321–337.
Boyce, J.W., Liu, Y., Rossman, G.R., Guan, Y.B., Eiler, J.M., Stolper, E.M., Taylor, L.A., 2010. Lunar apatite with terrestrial volatile abundances. Nature 466 466-462.
Bygden, J., Sichen, D., Seetharaman, S., 1994. A thermodynamic study of the molybdenum–oxygen system. Metal. Trans. B 25, 885–891.

Campbell, A.J., Danielson, L., Righter, K., Seagle, C.T., Wang, Y., Prakapenka, V.B., 2009. High pressure effects on the iron–iron oxide and nickel–nickel oxide oxygen fugacity buffers. Earth Planet Sci. Lett. 286, 556–564.
Carroll, M.R., Stolper, E.M., 1993. Noble-gas solubilities in silicate melts and glasses – new experimental results for argon and the relationship between solubility and ionic porosity. Geochim. Cosmochim. Acta 57, 5039–5051.
Corgne, A., Keshav, S., Wood, B.J., McDonough, W.F., Fei, Y.W., 2008. Metal-silicate partitioning and constraints on core composition and oxygen fugacity during Earth accretion. Geochim. Cosmochim. Acta 72, 574–589.
Delano, J.W., 2001. Redox history of the Earth's interior since similar to 3900 Ma: Implications for prebiotic molecules. Origin Life Evol. Biosphys. 31, 311–341.
Drake, M.J., 2005. Origin of water in the terrestrial planets. Meteor. Planet. Sci. 40, 1–9.
Duman, E., et al., 2004. Large spontaneous magnetostrictive softening below the Curie temperature of Fe_3C invar particles. J. Appl. Phys. 96, 5668–5672.
Elkins-Tanton, L., Grove, T.L., 2011. Water (hydrogen) in the lunar mantle: results from petrology and magma ocean modeling. Earth Planet. Sci. Lett. 307, 173–179.
Epicier, T., Dubois, J., Esnouf, C., Fantozzi, G., 1988. Neutron powder diffraction studies of transition metal hemicarbides M_2C_{1-x} – II. In situ high temperature study on W_2C_{1-x} and Mo_2C_{1-x}. Acta Metall. 36, 1903–1921.
Eugster, H.P., Wones, D.R., 1962. Stability relations of the ferruginous biotite, annite. J. Petrol. 3, 82–125.
Fluegel, A., 2007. Global model for calculating room-temperature glass density from the composition. J. Am. Ceram. Soc. 9, 2622–2625.
Fried, L.E., Howard, W.M., Souers, P.C., 2002. EXP6: a new equation of state library for high pressure thermochemistry. In: Proceedings of 12th International Detonation Symposium.
Frost, D.J., Liebske, C., Langenhorst, F., McCammon, C.A., Tronnes, R.G., Rubie, D.C., 2004. Experimental evidence for the existence of iron-rich metal in the Earth's lower mantle. Nature 428, 409–412.
Frost, D.J., McCammon, C.A., 2008. The redox state of Earth's mantle. Ann. Rev. Earth Planet. Sci. 36, 389–420.
Frost, D.J., Mann, U., Asahara, Y., Rubie, D.C., 2008. The redox state of the mantle during and just after core formation. Philos. Trans. R. Soc. A 366, 4315–4337.
Fukai, Y., 1984. The iron–water reaction and the evolution of the Earth. Nature 308, 174–175.
Gaillard, F., Schmidt, B., Mackwell, S., McCammon, C., 2003. Rate of hydrogen-iron redox exchange in silicate melts and glasses. Geochim. Cosmochim. Acta 67 2427-2421.
Genda, H., Ikoma, H., 2008. Origin of the ocean on the Earth: early evolution of water D/H in a hydrogen-rich atmosphere. Icarus 194, 42–52.
Ghiorso, M.S., Hirschmann, M.M., Reiners, P.W., Kress, V.C., 2002. The pMELTS: A revision of MELTS for improved calculation of phase relations and major element partitioning related to partial melting of the mantle to 3 GPa. Geochem. Geophys. Geosyst. 3 #2001GC000217.
Greaves, J.S., 2005. Disks around stars and the growth of planetary systems. Science 307, 68–71.
Greenwood, J.P., Itoh, S., Sakamoto, N., Warren, P., Taylor, L., Yurimoto, H., 2011. Hydrogen isotope ratios in lunar rocks indicate delivery of cometary water to the Moon. Nat. Geosci. 4, 79–82.
Guillot, B., Sator, N., 2012. Noble gases in high pressure silicate liquids: A computer simulation study. Geochim. Cosmochim. Acta 80, 51–69.
Haines, J., Leger, J.M., Chateau, C., Lother, J.E., 2001. Experimental and theoretical investigation of Mo_2C at high pressure. J. Phys.: Condens. Matter 13, 2447.
Hallstedt, B., Djurovic, D., Von Appen, J., Dronskowski, R., Dick, A., Körmann, F., Hickel, T., Neugebauer, J., 2010. Thermodynamic properties of cementite (Fe_3C). Calphad 34, 129–133.
Hanfland, M., Beister, H., Syassen, K., 1989. Graphite under pressure: equation of state and first-order Raman modes. Phys. Rev. B, 12598–12603.
Hashimoto, G.L., Abe, Y., Sugita, S., 2007. The chemical composition of the early terrestrial atmosphere: formation of a reducing atmosphere from CI-like material. J. Geophys. Res. 112, E0501.
Hauri, E.H., Weinreich, T., Saal, A.E., Rutherford, M.C., Van Orman, J.A., 2011. High pre-eruptive water contents preserved in lunar melt inclusions. Science 333, 213–215.
Hirschmann, M.M., 2006. Water, melting, and the deep Earth H_2O cycle. Ann. Rev. Earth Planet. Sci. 34, 629–653.
Hirschmann, M.M., 2012. Magma ocean influence on early atmosphere mass and composition. Earth Planet. Sci. Lett., 341-344, 48–57, http://dx.doi.org/10.1016/j.epsl.2012.06.015.
Hirschmann, M.M., Aubaud, C., Withers, A.C., 2006. Petrologic structure of a hydrous 410 km discontinuity. In: Earth's Deep Water Cycle, AGU Monograph, vol. 168, pp. 277–288.
Holloway, J.R., Blank, J.G., 1994. Application of experimental results to C–O–H species in natural melts. In Volatiles In Magmas. Rev. Mineral 30, 187–230.
Ikoma, M., Genda, H., 2006. Constraints on the mass of a habitable planet with water of nebular origin. Astrophys. J. 648, 695–706.
Iwai, T., Takahashi, I., Handa, M., 1986. Gibbs free energies of formation of molybdenum carbide and tungsten carbide from 1173 to 1573 K. Metall Trans. A 17, 2031–2034.
Jakobsson, S., Holloway, J.R., 2008. Mantle melting in equilibrium with an iron–wustite–graphite buffered COH-fluid. Contrib. Mineral. Petrol. 155, 247–256.
Kadik, A.A., Kurovskaya, N.A., Ignat'ev, Y.A., Kononkova, N.N., Koltashev, V.V., Plotnichenko, V.G., 2011. Influence of oxygen fugacity on the solubility of nitrogen, carbon, and hydrogen in $FeO–Na_2O–SiO_2–Al_2O_3$ melts in equilibrium with metallic iron at 1.5 GPa and 1400 °C. Geochem. Int. 49, 429–438.
Kadik, A., Pineau, F., Litvin, Y., Jendrzejewski, N., Martinez, I., Javoy, M., 2004. Formation of carbon and hydrogen species in magmas at low oxygen fugacity. J. Petrol. 45, 1297–1310.
Karner, J.M., Sutton, S.R., Papike, J.J., Shearer, C.K., Jones, J.H., Newville, M., 2006. Application of a new vanadium valence oxybarometer to basaltic glasses from the Earth, Moon, and Mars. Am. Mineral. 91, 270–277.
Kuramoto, K., Matsui, T., 1996. Partitioning of H and C between the mantle and core during the core formation in the Earth: Its implications for the atmospheric evolution and redox state of early mantle. J. Geophys. Res. 101, 14909–14932.
Li, J., Agee, C.B., 1996. Geochemistry of mantle-core differentiation at high pressure. Nature 381, 686–689.
Longhi, J., 1992. Experimental petrology and petrogenesis of mare volcanics. Geochim. Cosmochim. Acta 56, 2235–2251.
Lowitzer, S., Winkler, B., Tucker, M., 2006. Thermoelastic behavior of graphite from in situe high pressure high temperature neutron diffraction. Phys. Rev. B., 214115.
Luth, R.W., Mysen, B.O., Virgo, D., 1987. Raman-spectroscopic study of the solubility behavior of H_2 in the system $Na_2O–Al_2O_3–SiO_2–H_2$. Am. Mineral. 72, 481–486.
Matsukage, K.N., Jing, Z., Karato, S.-I., 2005. Density of hydrous silicate melt at the conditions of Earth's deep upper mantle. Nature 438, 488.
McCubbin, F.M., Steel, A., Hauri, E.H., Nekvasil, H., Yamashita, S., Hemley, R.J., 2010a. Nominally hydrous magmatism on the Moon. Proc. Nat. Acad. Sci. USA 107, 11223–11228.
McCubbin, F.M., Smirnov, A., Nekvasil, H., Wang, J.H., Hauri, E., Lindsley, D.H., 2010b. Hydrous magmatism on Mars: a source of water for the surface and subsurface during the Amazonian. Earth Planet. Sci. Lett. 292, 132–138.
Moore, G.M., Venneman, T., Carmichael, I.S.E., 1998. An empirical model for the solubility of water in magmas to 3 kbar. Am. Mineral. 83, 36–42.
Mysen, B.O., Kumamoto, K., Cody, G.D., Fogel, M.L., 2011. Solubility and solution mechanisms of C–O–H volatiles in silicate melt with variable redox conditions and melt composition at upper mantle temperatures and pressures. Geochim. Cosmochim. Acta 75, 6183–6199.
Nuccio, P.M., Paonita, A., 2000. Investigation of the noble gas solubility in $H_2O–CO_2$ bearing silicate liquids at moderate pressure II: the extended ionic porosity (EIP) model. Earth Planet. Sci. Lett. 183, 499–512.
Ochs, F.A., Lange, R.A., 1999. The density of hydrous magmatic liquids. Science 283, 1314–1317.
Ohlhorst, S., Behrens, H., Holtz, F., 2001. Compositional dependence of molar absorptivities of near-infrared OH and H2O bands in rhyolitic to basaltic glasses. Chem. Geol. 174, 5–20.
Ohtani, E., Hirao, N., Kondo, T., Ito, M., Kikegawa, T., 2005. Iron–water reaction at high pressure and temperature, and hydrogen transport into the core. Phys. Chem. Mineral. 32, 77–82.
Okuchi, T., 1997. Hydrogen partitioning into molten iron at high pressure: Implications for Earth's core. Science 278, 1781–1784.
O'Neill, H.S.C., 1988. Systems Fe–O and Cu–O: thermodynamic data for the equilibria Fe-''FeO'', Fe–Fe_3O_4, ''FeO''- Fe_3O_4 Fe_3O_4–Fe_2O_3, Cu–Cu_2O and Cu_2O–CuO from emf measurements. Am. Mineral. 73, 470–486.
Raymond, S.N., O'Brien, D.P., Morbidelli, A., Kaib, N.A., 2009. Building the terrestrial planets: constrained accretion in the inner Solar System. Icarus 203, 644–662.
Rohrbach, A., Ballhaus, C., Golla-Schindler, U., Ulmer, P., Kamenetsky, V.S., Kuzmin, D.V., 2007. Metal saturation in the upper mantle. Nature 449, 456–458.
Rubie, D.C., Frost, D.J., Mann, U., Asahara, Y., Nimmo, F., Tsuno, K., Kegler, P., Holzheid, A., Palme, H., 2011. Heterogeneous accretion, composition and core-mantle differentiation of the Earth. Earth Planet. Sci. Lett. 301, 31–42.
Saal, A.E., Hauri, E.H., Lo Cascio, M., Van Orman, J.A., Rutherford, M.C., Cooper, R.F., 2008. Volatile content of lunar volcanic glasses and the presence of water in the Moon's interior. Nature 454 192-U138.
Sakamaki, T., Suzuki, A., Ohtani, E., 2006. Stability of hydrous melt at the base of the Earth's upper mantle. Nature 439, 192–194.
Sato, M., 1976. Oxygen fugacity and other thermochemical parameters of Apollo 17 high-Ti basalts and their impilcations on the reduction mechanism. In: Proceedings of the 7th Lunar Science Conference, pp. 1323–1344.
Schaefer, L., Fegley, B., 2007. Outgassing of ordinary chondritic material and some of its implications for the chemistry of asteroids, planets, and satellites. Icarus 186, 462–483.
Schmidt, B.C., 1998. Incorporation of H_2 in vitreous silica, qualitative and quantitative determination from Raman and infrared spectroscopy. J. Non-crystall. Solids 240, 91–103.
Shang, L., Chou, I.M., Lu, W., Burruss, R.C., Zhang, Y., 2009. Determination of diffusion coefficients of hydrogen in fused silica between 296 and 523 K by Raman spectroscopy and application of fused silica capillaries in studying redox reactions. Geochim. Cosmochim. Acta 73, 5435–5443.
Shannon, R.D., 1976. Revised effective ionic radii and systematic studies of interatomic distances in halides and chalcogenides. Acta Crystallogr. A32, 751–767.
Sharma, S.K., Mao, H.K., Bell, P.M., 1979. Raman study of n-H_2, under very high pressures at room temperature. Carnegie Institution of Washington, Year Book, vol. 78,pp. 645-649.
Shelby, J.E., 1994. Protonic species in vitreous silica. J. Non-Crystal. Solids 179, 138–147.
Stevenson, D.J., 1977. Hydrogen in Earth's core. Nature 268, 130–131.
Tauzin, B., Debayle, E., Wittinger, G., 2010. Seismic evidence for a global low-velocity layer within the Earth's upper mantle. Nat. Geosci. 3, 718–721.

Taylor, W.R., Green, D.H., 1988. Measurement of reduced peridotite-C–O–H solidus and implications for redox melting of the mantle. Nature 332, 349–352.
Tenner, T.J., Hirschmann, M.M., Withers, A.C., Hervig, R.L., 2009. Hydrogen partitioning between nominally anhydrous upper mantle minerals and melt between 3 and 5 GPa. Chem. Geol. 262, 42.
Trail, D., Watson, E.B., Tailby, N.T., 2011. The oxidation state of Hadean magmas and implications for early Earth's atmosphere. Nature 480, 79–82.
Wadhwa, M., 2008. Redox conditions on small bodies, the Moon and Mars. Oxygen in the Solar System Rev. Mineral. Geochem. 68, 493–510.
Weitz, C.M., Rutherford, M.J., Head, J.W., 1997. Oxidation states and ascent history of the Apollo 17 volcanic beads as inferred from metal-glass equilibria. Geochim. Cosmochim. Acta 61, 2765–2775.
Williams, Q., Hemley, R.J., 2001. Hydrogen in the deep Earth. Ann. Rev. Earth. Planet. Sci. 29, 365–418.
Withers, A.C., Behrens, H., 1999. Temperature-induced changes in the NR spectra of hydrous albitic and rhyolitic glasses between 300 and 100 K. Phys. Chem. Mineral 27, 119–132.
Wood, B.J., 1993. Carbon in the core. Earth Planet. Sci. Lett.. 117, 593–607.
Wood, B.J., Walter, M.J., Wade, J., 2006. Accretion of the Earth and segregation of its core. Nature 441, 825–833.
Wood, I.G., et al., 2004. Thermal expansion and crystal structure of cementite, Fe3C, between 4 and 600 K determined by time-of-flight neutron powder diffraction. J. Appl. Crystallogr. 37, 82–90.
Xirouchakis, D., Hirschmann, M.M., Simpson, J., 2001. The effect of titanium on the silica content of mantle-derived melts. Geochim. Cosmochim. Acta 65, 2029–2045.
Zhang, C., Duan, Z., 2009. A model for C–O–H fluid in the Earth's mantle. Geochim. Cosmochim. Acta 73, 2089–2102.
Zhao, Y., Lawson, A.C., Zhang, J., Bennett, B.I., Von Dreele, R.B., 2000. Thermoelastic equation of state of molybdenum. Phys. Rev. B 62, 8766–8776.